IN-SITU X-RAY MONITORING OF DAMAGE ACCUMULATION IN SIC/RBSN TENSILE SPECIMENS

George Y. Baaklini
National Aeronautics and Space Administration
Lewis Research Center
Cleveland, Ohio 44135

and

Ramkrishna T. Bhatt
Propulsion Directorate
U.S. Army Aviation Research and Technology Activity-AVSCOM
Lewis Research Center
Cleveland, Ohio 44135

ABSTRACT

The room-temperature tensile testing of silicon carbide fiber-reinforced reaction-bonded silicon nitride (SiC/RBSN) composite specimens was monitored by using in-situ x-ray film radiography. Radiographic evaluation before, during, and after loading provided data on the effect of preexisting volume flaws (high density impurities and local density variations) on the fracture behavior of composites. Results from $[0]_1$, $[0]_3$, $[0]_5$, and $[0]_8$ composite specimens, showed that x-ray film radiography can monitor damage accumulation during tensile loading. Matrix cracking, fiber-matrix debonding, and fiber pullout were imaged throughout the tensile loading history of the specimens. Further, in-situ film radiography was found to be a helpful and practical technique for estimating interfacial shear strength between the SiC fiber and the RBSN matrix by the matrix crack spacing method. It is concluded that pretest, in-situ, and post-test radiography can provide for a greater understanding of ceramic matrix composite mechanical behavior, a verification of related experimental procedures, and a validation and development of related analytical models.

INTRODUCTION

Ceramic matrix composite (CMC) systems are being developed for heat engine applications.[1-3] The ultimate goal of current research is understanding of composite behavior in order to better optimize the composite properties for different hot section applications. CMC's are being developed because they provide enhanced

material toughness while maintaining the useful properties of monolithic ceramics. The fiber-matrix interface in CMC's plays an important role in determining toughness-related properties,[4,5] but there is very little quantitative data on interface properties.[4] Further, composite failure processes are not well understood because of a lack of reliable data.

In order to use CMC's more effectively, their failure processes and damage tolerances must be understood and, in turn, their failure analysis and mechanics models must be improved. Methodologies such as in-situ x-ray radiography and in-situ acoustic emission tests can help in imaging and sensing, respectively, the failure sequences and damage accumulation in composite specimens under loading.[6,7] The information gathered from such in-situ monitoring can help in the development and validation of analytical models, and in coordinating between experiment and theory. Damage and failure mechanisms, e.g., transverse matrix cracking, fiber-matrix debonding, fiber breaking, fiber pullout, and delamination can be better understood if imaged and/or identified as they occur. Such in-situ examination will help identify and clarify the sequence in which these mechanisms take place, and consequently aid in identification of deformation controlling properties, i.e., whether they are matrix dominated properties, fiber dominated properties, or a combination of both.

The objectives of this study are to demonstrate the capabilities of in-situ x-ray radiography in monitoring damage accumulation and failure processes in unidirectionally reinforced SiC/RBSN system under tensile loading, and consequently, to determine the interfacial shear strength between the SiC fiber and the RBSN matrix. The major benefits of this research are: better interpretation of mechanical test results, validation of analytical models, verification of experimental procedures, and optimimization of the fabrication process.

EXPERIMENTAL

In-situ X-ray and Materials Testing System

An in-situ x-ray and materials testing system (IX-MTS) facility was built in order to conduct in-situ x-ray monitoring of materials under loading. Figure 1 shows a schematic diagram of the experimental set-up. Figures 2 and 3 show the IX-MTS and a close-up of the specimen testing/evaluation region. The IX-MTS consisted of an 3.2 kW x-ray system, and a electro-mechanical materials testing system.

The x-ray system was capable of reaching 160 kV or 45 mA with either a 400 μm or a 3 mm focal spot size. Film radiography was the detection medium chosen because of its high resolution and registration capabilities. The materials testing system[*] consisted of a 250 kN load frame, a 100 kN electric-actuator, a 50 kN load cell, and a digital control system.

The room-temperature tensile testing was done in load control for some specimens and in displacement control for others. Loading and displacement rates were 4.54 kg/min and 25 μm/min, respectively. These relatively slow rates were used in order to perform in-situ film radiographic monitoring without holding the load or displacement. The load did not change by more than 10 kg during the radiographic exposure (25 to 35 sec) except at failure. As the tensile specimen was pulled, the axial strains were monitored by two adhesively bonded strain gauges and a clip-on extensometer. Two x-ray films were exposed at different stress-strain levels during the test.

The strain gauges were bonded to the faces of the specimen and the extensometer was clipped to the edge while leaving the 2.54 cm gauge length accessible to in-situ radiography. Immediately after the test, the specimen was evaluated with microfocus radiography and optical metallography. Films were then developed and radiographic images were made to interpret the results in conjunction with the stress-strain data.

---

[*]Instron Materials Testing System, Canton, Massachusetts.

Radiographic Evaluation

Two different x-ray systems were used: (1) a conventional system (conventionally designed x-ray tube) with a 400 μm focal spot size and (2) a microfocus system with a 10 μm focal spot size. Conventional radiographs were made in a direct contact mode (image is 100 percent of object) while microfocus radiographs were made in a projection mode with a resultant magnified radiographic image.

Conventional radiography was used to evaluate silicon powder cloths and composite panels before and after machining. Microfocus radiography was used to evaluate the tensile specimens before loading and after failure because of its high resolution capabilities.[8]

Specimens

The SiC/RBSN composite panels, $[0]_1$, $[0]_3$, $[0]_5$, and $[0]_8$, were produced by conventional ceramic powder fabrication methods[9] using 142 μm diameter SiC fibers, designated as double coated SCS-6 fibers.[**] Reference 10 describes the method of preparing fiber-reinforced ceramic materials in details.

The radiographic evaluation of machined panels guided the choice of cutting tensile specimens with different density features from the composite panels: (1) specimens with sizeable volumetric high density impurity located in the gauge length region, (2) specimens with many small high density impurities in the gauge length region, and (3) specimens with low density variations were chosen. Specimen dimensions were 125 by 12.7 by 1 to 2.0 mm. The fiber volume fractions were 9, 16, 19, and 24 percent. Two axial wire-wound strain gauges were adhesively bonded to the front and back faces of each tensile specimen which had glass fiber-reinforced epoxy tabs.

[**]Textron Specialty Materials Division, Lowell, Massachusetts.

Radiographic Characterization Prior To Testing

Figure 4 shows the radiographic image of a typical $[0]_3$ SiC/RBSN panel before and after machining the graphite layer. The graphite layer formed during the high temperature vacuum hot pressing composite fabrication. It is obvious from the radiographic print before machining that the graphite layer masks any density variation information from the SiC/RBSN panel, i.e., the density variation detected was mainly due to variation in the thickness and density of the graphite layer itself.

After machining the graphite layer, radiographic characterization of the composite panels was possible. The fiber architecture was detected, for example, the orientation of the fibers as evident in Fig. 4, and fiber bunching and misalignment in other panels (not shown) were detected. High density impurities, i.e., the dark isolated features (black dots) which are shown in Fig. 4(b), were chemically identified as iron rich inclusions. Figure 4(b) also shows localized low density (light to white) due to surface chipping.

Mechanical Properties

The room temperature tensile stress-strain behavior for the $[0]_1$, $[0]_3$, $[0]_5$, and $[0]_8$ SiC/RBSN are shown in Fig. 5, and corresponding tensile property data are listed in Table I. The values of the rule of mixtures composite modulus,[11] $E_{(rom)c}$, which is given by

$$E_{(rom)c} = E_m V_m + E_f V_f \qquad (1)$$

where E is modulus, V is volume fraction, and c, f, and m refer to composite, fiber, and matrix, are given in Table I. The E_m and E_f values used were 390 MPa and 110 MPa respectively.[9]

The stress-strain results for the $[0]_1$ and the $[0]_3$ showed a linear behavior until final fracture. At the ultimate stress the specimens which were tested in the

load control mode failed catastrophically. Specimens tested in the displacement control mode showed load dropping region before final failure. Radiography showed that in this region fiber pullout was the dominant failure mechanism.

The stress-strain results for the $[0]_5$ specimens showed three distinct regions. In the initial region the stress varied linearly with the strain up to an average stress level of 197 MPa when the load momentarily dropped. In the second region the stress strain curve became nonlinear and displayed serrations due to load dropping and recovering without exceeding an average engineering stress of 226 MPa. The third region showed a fiber pullout behavior where load was dropping but not as catastrophically as at the final failure.

The stress-strain results for the $[0]_8$ specimen showed three distinct regions. In the initial region, the stress varied linearly with the strain up to a stress level of approximately 195 MPa when matrix cracking was evident. In the second region the behavior was nonlinear where load was either holding or dropping then recovering and increasing as the strain was increasing. In the third region, the stress varied linearly with the strain in segments where modulus was either the same or decreasing until maximum tensile stress was reached, thereafter the specimen showed minor load carrying capacity before it finally fractured.

In-situ Radiographic Imaging

Figure 6 shows microfocus radiographs of $[0]_1$ specimen. These radiographs were taken before loading the specimen and after it failed. The before-loading image shows a subsurface 0.5 by 1.0 mm high density impurity. This high density region consisted of a cluster of 50 μm diameter inclusions. The after-failure image shows that the fracture initiated at the site of the impurity and propagated across the width of the sample. This was inferred from the size and number of the fiber pullouts seen. A closer look at the radiographic film showed the presence of multiple breakages per fiber. Figure 6(c) shows that microfocus radiography detects 40 μm fiber pullout.

6

Figure 7(a) and (b) show microfocus radiographs of two different $[0]_1$ specimens after failure. These radiographs show random fibers pullout and multiple matrix cracks. These cracks did not propagate through the thickness of the specimens because of fiber-matrix debonding at the fiber-matrix interface. Similarly, in Fig. 7(c), $[0]_3$, through-width but not through-thickness cracks, fibers pullout, and fiber-matrix debonding are present. The white region near the right of Fig. 7(c) is an indication of extensive fiber-matrix debonds which has also occurred outside the 2.54 cm gauge length (the area between the two bonded strain gauges).

Figure 8 shows three radiographs R6, R8, and R10 selected out of a series of 10 in-situ radiographs taken throughout the tensile loading history of a $[0]_5$ specimen. The stress-strain behavior is also shown. In Fig. 8, although radiographs were made at R3, R4, and R5 they did not show the presence of matrix cracking. R6 shows one major through-width crack. R8 shows multiple cracks. R10, taken after failure shows the resulting fibers pullout, the closure of the cracks imaged earlier, and the major cracks with corresponding fiber-matrix debonds region at failure. Radiographs for R7 and R9 show similar information but they were not included because of space limitations in Fig. 8.

Figure 9 shows selected in-situ radiographs made during tensile loading history of a $[0]_8$ specimen. R0 is a radiographic print of the specimen at near 0 kg load. R8 is a radiographic print of the specimen at 268 MPa and 0.2 percent strain. This radiograph, R8, shows 6 cracks perpendicular to the fiber orientation, propagating from right to left but not all the way through the width of the specimen. Figure 10 and Table II present a detailed summary of the crack development and corresponding spacing data imaged in R8. Radiographs R9 and R10 in Fig. 9 show 10 through-thickness and through-width matrix cracks at 410 and 538 MPa, respectively.

Figure 11 is a schematic of the matrix crack spacing method for calculation of estimated interfacial shear strength, T_f based on the Aveston , Cooper, and Kelly (ACK) theory[12]

$$\tau_f = \frac{\sigma_c^m D_f}{2.98\,(\overline{X})\,V_f(1 + E_f V_f/E_m V_m)} \qquad (2)$$

where σ_c^m is the composite stress corresponding to the first matrix crack, $\overline{X}$ is the mean crack spacing, D_f is the fiber diameter, and the rest of the terms are as defined earlier in Eq. (1). For $[0]_8$ with, 24 percent fiber volume fraction, 3.56 mm mean crack spacing, 195 MPa composite stress at first matrix crack, 390 MPa fiber modulus, and 110 MPa matrix modulus the interfacial shear strength was calculated from Eq. (2) to be 5 MPa.

DISCUSSION

Significance of Radiographic Characterization

The radiographic results of silicon powder cloths and SiC/RBSN panels helped identify: (1) the presence and type of impurities, and (2), the local density variations within each panel and between panels. This information presented options in designing the tensile specimens from the panels. Specimens that contained large volumetric flaws can be monitored and compared with specimens that were free of these flaws. Specimens that contained excessive local density variations can be compared with specimens that had minor local density variations. Consequently, based on whether or not impurities and local density variations are affecting the fracture behavior of the composite, materials engineers can modify powder processing or composite fabrication in order to free the composite from detrimental defects.

In this study, it was found that a 0.5 mm by 1.0 mm high density region can affect the fracture behavior of the $[0]_1$ composite (Fig. 6) because the latter is behaving more like monolithic with one linear region ending in a catastrophic failure at ultimate stress (Fig. 5). However, isolated and randomly distributed high density inclusions less than 150 μm in diameter did not directly affect the fracture behavior

8

of the $[0]_1$ and $[0]_3$ composite specimens. Similarly high density inclusions up to 225 μm in diameter did not affect the fracture behavior of the $[0]_5$ composite specimens. Local density variations within the tensile specimens did not seem to affect the fracture behavior of the composite. These are preliminary conclusions based on the limited number of samples that have been monitored and tested.

Microfocus radiography of failed specimens proved useful in detecting fibers pullout. Cracks and crack branchings that had not closed after failure were imaged. This shows advantages of microfocus over conventional radiography in studying and explaining the behavior of composites under load.

Mechanical Properties

The primary modulus, before first matrix cracking of the composite, E_{pc}, was about the same, within 12 percent, for all $[0]_1$, $[0]_3$, $[0]_5$ and $[0]_8$ composite specimens. These primary moduli either overestimated by 12 percent or came close to 1 percent of the corresponding rule of mixtures composite modulus, $E_{(rom)c}$, defined in Eq. (1). This overestimate can be explained by the fact that one-ply, three-ply, and five-ply materials were thinner and hence denser than the normal RBSN matrix where a modulus of 110 MPa is expected. The fact that, E_{pc}'s are close to $E_{(rom)c}$'s, is indicative of an adequate load transfer between fibers and matrix.[13]

The first matrix cracking strains and stresses of $[0]_1$, and $[0]_3$ were also the strain-to-failure values and the ultimate strengths of these specimens, respectively. In contrast, first matrix stress and strain for $[0]_5$ (19 percent volume fraction) were very close to those of $[0]_8$ (24 percent volume fraction), where the strain to failure showed great enhancement over the one-ply, the three-ply, and the ⌐-ply composite specimens.

The ultimate tensile strength increased with the fiber volume fraction of all composite specimens because it is primarily controlled by the bundle strength of the fibers.[13]

Significance of In-situ Radiography

In the case of $[0]_1$ and $[0]_3$ composites, in-situ radiography was able to immediately image cracks and fiber pullout after failure occurred at ultimate strength. This was only achieved when the samples were tested in displacement control. Under load control catastrophic failure occurring at ultimate strength prevents the operator from making an x-ray exposure. In-situ radiography during failure and in-situ and microfocus radiography immediately after failure helped identify the presence and location of non transparent matrix cracks on the ply level, of nontransparent fiber pullout, and of fiber matrix debonding.

In the case of $[0]_5$, failure sequences were radiographically imaged in the non-linear region, and during and after the fiber pullout region (Fig. 8). Breakages of fibers can not be imaged until fibers start pulling apart. Microcracks which may have existed in the linear region, can not be imaged because of limitations in the resolution and the detection capabilities of the x-ray system. The first matrix crack was imaged after the stress-strain curve had indicated that matrix cracking occurred. Thereafter, multiple cracks were imaged as the specimen was strained, then fibers started to pull out and the matrix cracks started to close until the final failure of the composite. At this point major fiber pullout, fiber matrix debonding and fiber breakage were imaged. After failure, close optical examination demonstrated that matrix cracks had propagated across the width of the sample but not through the thickness.

In the case of $[0]_8$, in-situ radiography imaged matrix crack develop throughout the tensile loading history as shown in Figs. 9 and 10 and as summarized in Table II. In-situ radiography enabled the use of the mean crack spacing method to determine the interfacial shear strength as defined in Eq. (2), and also verified the usual experimental procedure[14] used to determine τ_f. From Table II and Fig. 9, it is apparent that the number of major matrix cracks and corresponding spacings have not changed between 71 and 93 percent of ultimate engineering strength. This

verifies that the procedure to unload the sample at about 75 percent[14] of ultimate

load to perform the crack spacing measurements under an optical microscope was done

in the proper loading region. This x-ray monitoring technique is ideal when compared

with its optical counterpart,[14] because, first stopping the test and unloading is not

practical. Second, estimating the presence of cracks which have already closed due

to unloading leads to an overestimate of τ_t. Third, the ultimate strength is real

not estimated from other similar samples. And fourth, if the sample shatters into

fragments after failure or fails earlier than expected the cracks have already been

imaged and spacings can be measured from the x-ray film. Further, even in-situ

optical monitoring will not deliver the above information; because the high

magnification needed to monitor the cracks reduces the imaging field and the working

focal length.

CONCLUSION

In-situ radiography of room temperature tensile testing of SCS-6 silicon

carbide fiber reinforced reaction-bonded silicon nitride (SiC/RBSN) composite

specimens is a good method for monitoring damage accumulation, and for determining

the interfacial shear strength between the SiC fiber and the RBSN matrix by the

matrix crack spacing method. Matrix cracking, fiber-matrix debonding, and fiber

pullout were imaged throughout the loading history of the specimens. Radiographic

evaluation before, after, and during loading provided data on the effect of

preexisting volume flaws, e.g., high density inclusions, and on the effect of local

density variations on the fracture behavior of composites. It is concluded that this

approach can provide a basis for interpretation of mechanical tests, for validation

of analytical models, and for verification of experimental procedures.

REFERENCES

[1]T. Mah, M.G. Mendiratta, A.P. Katz, and K.S. Mazdiyasni, "Recent Developments in

Fiber-Reinforced High-Temperature Ceramic Composites," Am. Ceram. Soc. Bull., 66

[2] 304-308 (1987).

[2]L. Heraud, P. Spriel, High Toughness C-SiC and SiC-SiC Composites in Heat Engines. Whisker- and Fiber-toughened Ceramics. R.A. Bradely, et al., eds., ASM International, pp. 217-224, 1988.

[3]R.T. Bhatt, The Properties of Silicon Carbide Fiber-Reinforced Silicon Nitride Composites. Whisker- and Fiber-Toughened Ceramics. R.A. Bradely, et al., eds, ASM International, pp. 199-208, 1988.

[4]R.J. Kerans, R.S. Hay, N.J. Pagano, and T.A. Parthasarathy, "The Role of the Fiber-Matrix Interface in Ceramic Composites," Am. Ceram. Soc. Bull., 68, pp. 429-442, 1989.

[5]A.G. Evans and D.B. Marshall, "The Mechanical Behavior of Ceramic Matrix Composites," Overview No. 85, Acta metall. 37, [10], pp. 2567-2583, 1989.

[6]G.Y. Baaklini, and R.T. Bhatt, "Preliminary x-ray monitoring of Damage Accumulation in SiC/RBSN," HITEMP Review-1990, NASA CP-10051, pp. 54-1 to 54-13.

[7]A. Chulya, G.Y. Baaklini, and R.T. Bhatt," Characterization of Damage and Fracture Mechanisms in Continuous Fiber-Reinforced SiC/RBSN Ceramic Matrix Composites," HITEMP Review-1990, NASA CP-10051, pp. 55-1 to 55-15.

[8]G.Y. Baaklini, and D.J. Roth, "Probability of Detection of Internal Voids in Structural Ceramics using Microfocus Radiography," J. Mater. Res., 1, [3], pp 457-467 May-June 1986.

[9]R.T. Bhatt, and R.E. Phillips, "Laminate Behavior for SiC Fiber-Reinforced Reaction-Bonded Silicon Nitride Matrix Composites," NASA TM-101350, 1988.

[10]R.T. Bhatt, "Method of Preparing Fiber-Reinforced Ceramic Materials," U.S. Pat. No. 4689188, 1987.

[11]B.D. Agarwal and L.J. Broutman, in Analysis and Performance of Fiber Composites, Chapter II, John Wiley & Sons, New York 1979.

[12]J. Aveston, G.A. Cooper, and A. Kelly, "Single and Multiple Fracture," in The Properties of Fiber Composites, Proceedings of the conference, pp. 15-26, IPC Science and Technology Press ltd., Surrey, England, 1971.

[13]R.T. Bhatt, "Influence of Interfacial Shear Strength on the Mechanical Properties of SiC Fiber Reinforced Reaction-Bonded Silicon Nitride Matrix Composites," NASA TM-102462, 1990.

[14]R.T. Bhatt, "Mechanical Properties of SiC Fiber-Reinforced Reaction-Bonded Si_3N_4 Composites," NASA TM-87085, 1985.

Table I.—Room temperature tensile property data for SiC/RBSN composite specimens.

SiC/RBSN	V_f, %	Number of specimens	E_c, GPa experimental	E_c^*, GPa rule of mixtures	σ, MPa ultimate	Proportional limit	
						σ, MPa	ε, %
[0]₁	9	5	160	135	129	129	0.08
[0]₃	16	1	178	155	178	178	0.10
[0]₅	19	3	180	163	226	197	0.11
[0]₈	24	1	175	177	576	195	0.12

* $E_c = E_m V_m + E_f V_f$ where $E_m = 110$ GPa & $E_f = 390$ GPa (ref. 9).

Table II.—Variation of crack density versus load for SiC-RBSN Composite ($V_f \approx 24\%$)

Radiograph number	Stress, MPa	Strain, %	% of ultimate (ult = 576 MPa)	Number of cracks detected by x-rays	Mean crack spacing, x, mm
R4	219	.14	38	1*	-
R5	226	.15	39	2*	-
R6	-	-	-	3*	8.56
R7	258	.18	45	5*	8.02
R8	268	.20	47	6*	6.42
R9	410	.40	71	10**	3.56
R10	538	.55	93	10**	3.56
R12	After failure			11**	3.47

* Not across - width cracks.
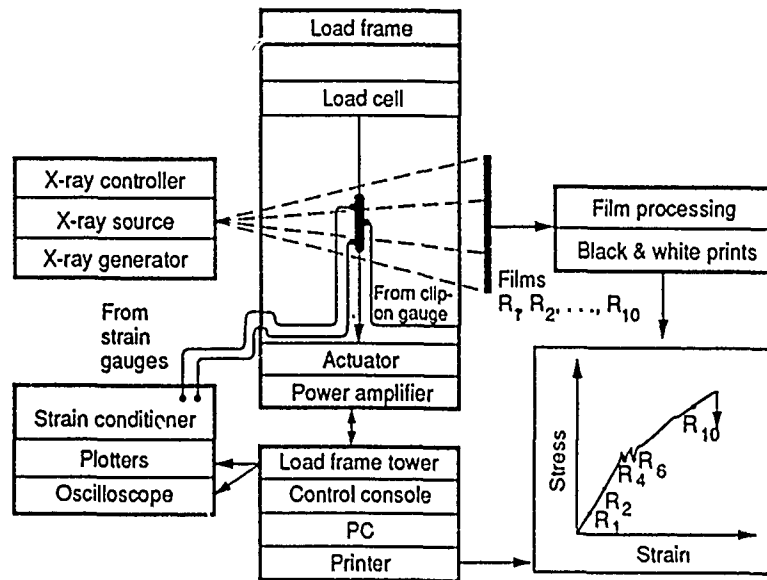** Across-width and through-thickness cracks.

Figure 1.—Schematic diagram of the In-situ x-ray and materials testing system.
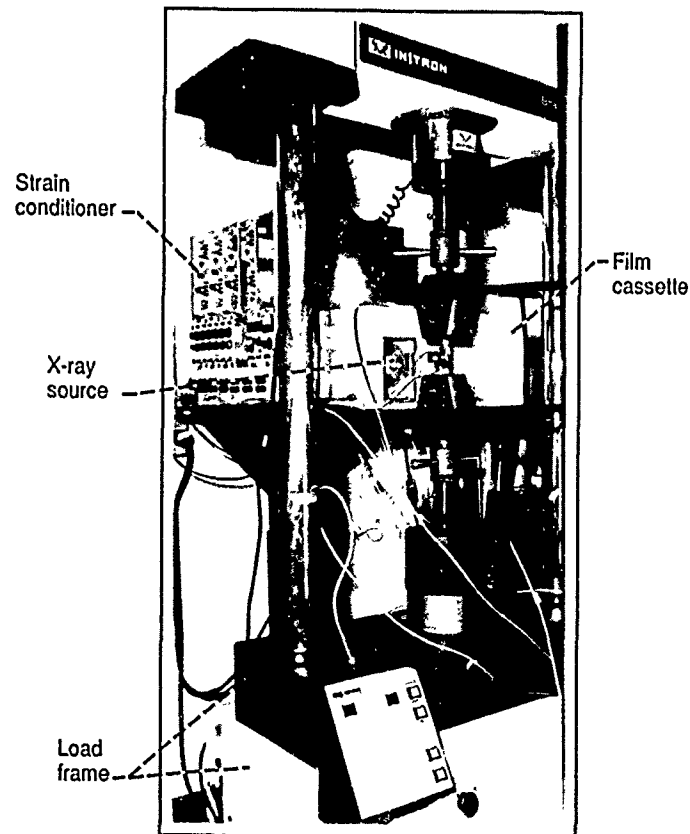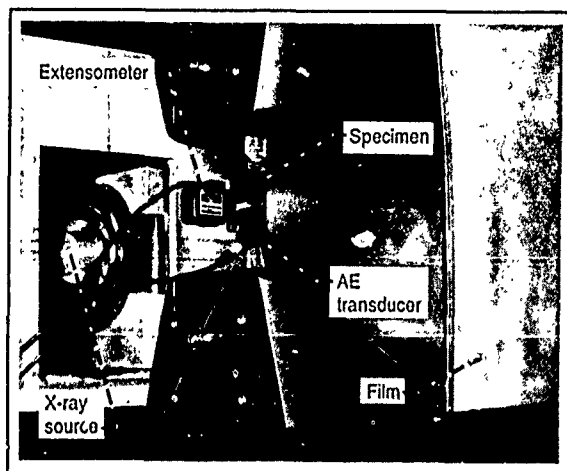

Figure 2.—In-Situ x-ray and materials testing system.

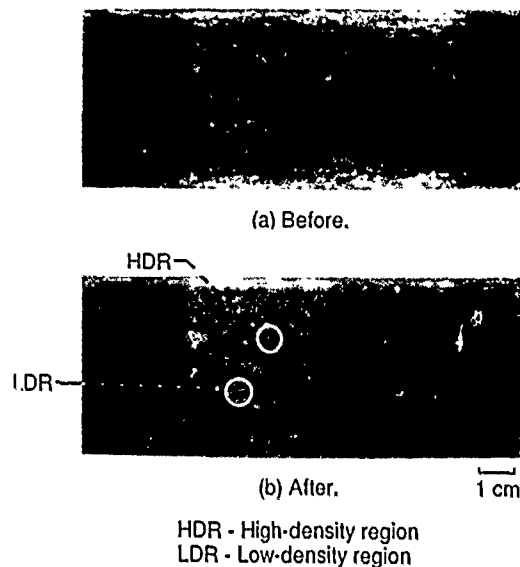Figure 3.—Detail of In-situ x-ray materials testing system.

(a) Before.

(b) After.

HDR - High-density region
LDR - Low-density region

Figure 4.—Conventional radiographs of $[0]_3$ panel before and after maching.
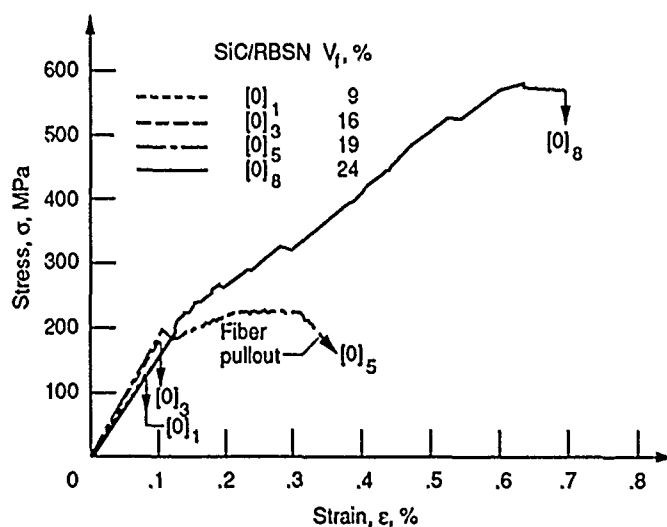
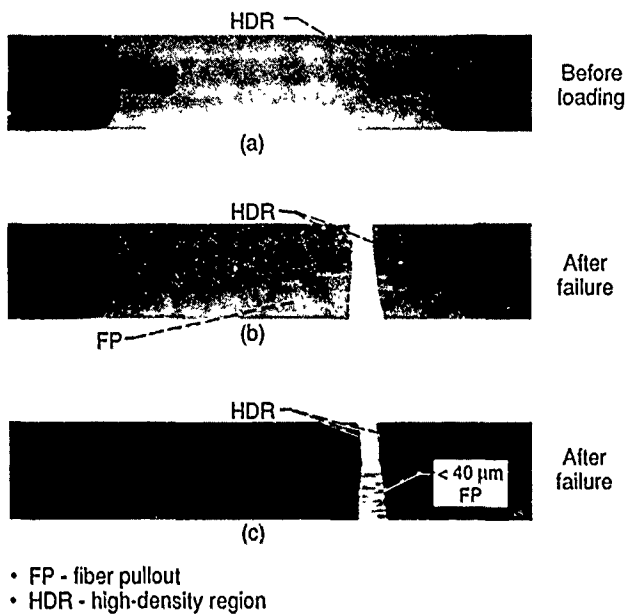Figure 5. Room temperature stress-strain behavior for uni-directionally reinforced SiC/RBSN composite specimens.

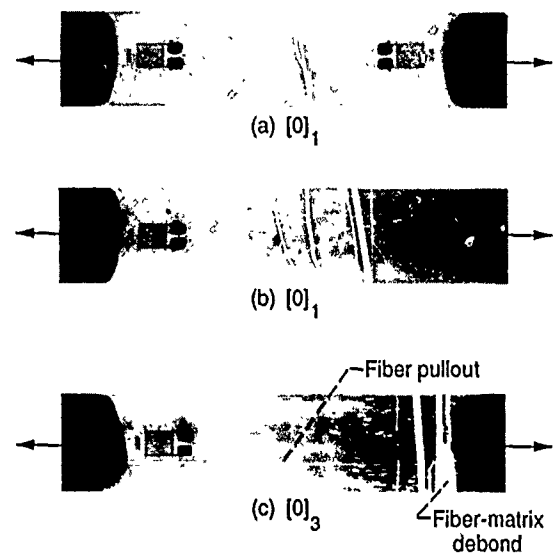Figure 6.—Microfocus radiographs of a $[0]_1$ SiC/RBSN specimen.

- FP - fiber pullout
- HDR - high-density region

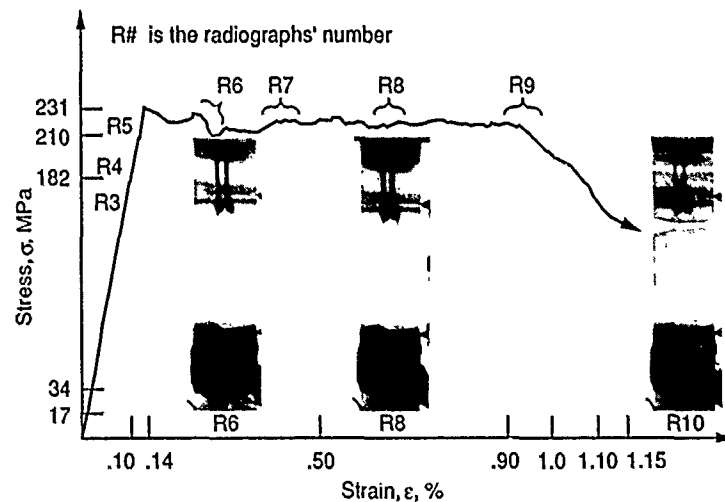Figure 7.- Microfocus radiographs of SiC/RBSN specimens after failure.

Figure 8.—Selected In-situ radiographs obtained during tensile loading of a $[0]_5$ SiC/RBSN composite ($V_f \approx 19\%$).
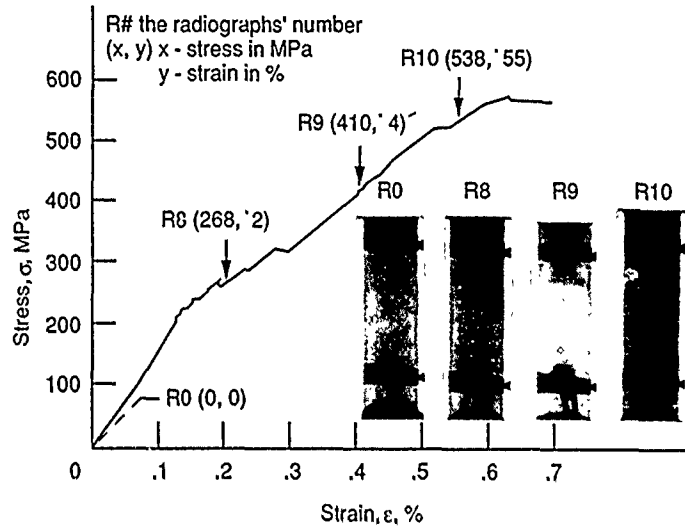
Figure 9.—Selected In-situ radiographs obtained during tensile loading of a $[0]_8$ SiC/RBSN composite ($V_f \approx 24\%$).
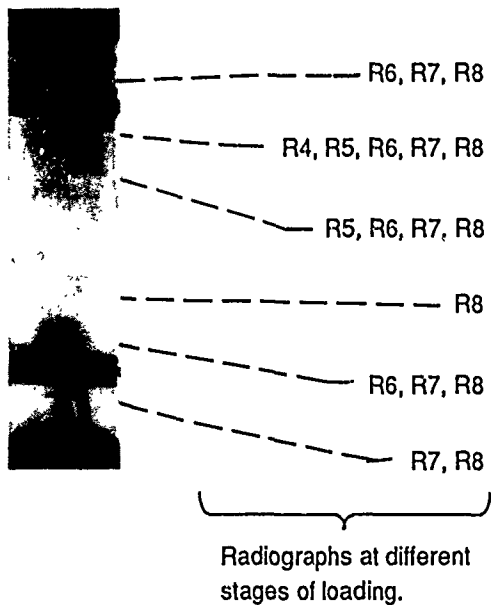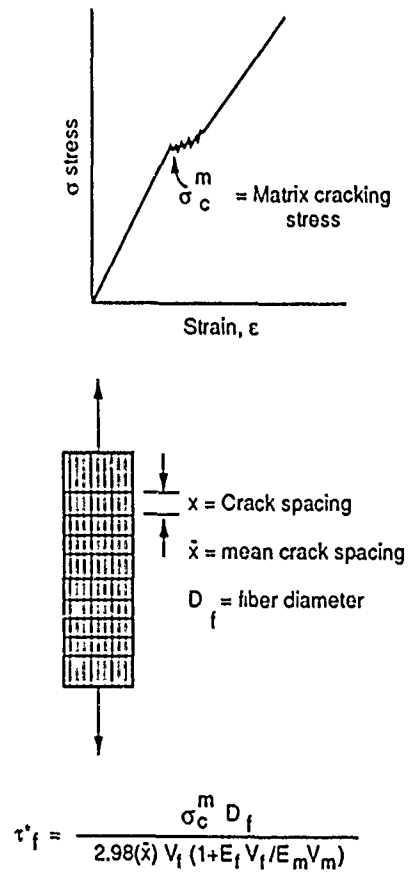

R6, R7, R8

R4, R5, R6, R7, R8

R5, R6, R7, R8

R8

R6, R7, R8

R7, R8

Radiographs at different stages of loading.

Figure 10.—Summary of resulting crack density as presented on radiograph number R8 at 268 MPa and 0.2% strain.

σ_c^m = Matrix cracking stress

x = Crack spacing

$\bar{x}$ = mean crack spacing

D_f = fiber diameter

$$\tau_f^* = \frac{\sigma_c^m \, D_f}{2.98(\bar{x}) \, V_f \, (1 + E_f V_f / E_m V_m)}$$

* Aveston, Cooper, and Kelly

Figure 11.—Matrix crack spacing method (τ_f).

NASA

National Aeronautics and
Space Administration

Report Documentation Page

1. Report No. NASA TM-103733 AVSCOM TR 90-C-019	2. Government Accession No.	3. Recipient's Catalog No.

4. Title and Subtitle	5. Report Date
In-Situ X-Ray Monitoring of Damage Accumulation in SiC/RBSN Tensile Specimens	
	6. Performing Organization Code

7. Author(s)	8. Performing Organization Report No.
George Y. Baaklini and Ramakrishna T. Bhatt	E-5971
	10. Work Unit No. 510-01-50 1L162211A47A

9. Performing Organization Name and Address	
NASA Lewis Research Center Cleveland, Ohio 44135-3191 and Propulsion Directorate U.S. Army Aviation Systems Command Cleveland, Ohio 44135-3191	11. Contract or Grant No.
	13. Type of Report and Period Covered

12. Sponsoring Agency Name and Address	
National Aeronautics and Space Administration Washington, D.C. 20546-0001 and U.S. Army Aviation Systems Command St. Louis, Mo. 63120-1798	Technical Memorandum
	14. Sponsoring Agency Code

15. Supplementary Notes

Prepared for the 15th Annual Conference on Composites and Advanced Ceramics, sponsored by the American Ceramic Society, Cocoa Beach, Florida, January 13-16, 1991. George Y. Baaklini, NASA Lewis Research Center; Ramakrishna T. Bhatt, Propulsion Directorate, U.S. Army Aviation Systems Command. Responsible person, George Y. Baaklini, (216) 433-6016.

16. Abstract

The room-temperature tensile testing of silicon carbide fiber reinforced reaction-bonded silicon nitride (SiC/RBSN) composite specimens was monitored by using in situ x-ray film radiography. Radiographic evaluation before, during, and after loading provided data on the effect of preexisting volume flaws (high density impurities, and local density variations) on the fracture behavior of composites. Results from $[0]_1$, $[0]_3$, $[0]_5$, and $[0]_8$ composite specimens, showed that x ray film radiography can monitor damage accumulation during tensile loading. Matrix cracking, fiber matrix debonding, and fiber pullout were imaged throughout the tensile loading history of the specimens Further, in situ film radiography was found to be a helpful and practical technique for estimating interfacial shear strength between the SiC fiber and the RBSN matrix by the matrix crack spacing method. It is concluded that pretest, in situ, and post test radiography can provide for a greater understanding of ceramic matrix composite mechanical behavior, a verification of related experimental procedures, and a validation and development of related analytical models.

17. Key Words (Suggested by Author(s))	18. Distribution Statement
X-Ray monitoring; Damage accumulation; Ceramic composites; HITEMP materials; NDE; Mechanical test; Failure processes; SiC; Si_3N_4; SiC/RBSN	Unclassified – Unlimited Subject Categories 24, 38 and 39

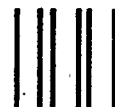| 19. Security Classif. (of this report) Unclassified	20. Security Classif. (of this page) Unclassified	21. No. of pages 18	22. Price* A03

National Aeronautics and
Space Administration

Lewis Research Center
Cleveland, Ohio 44135

FOURTH CLASS MAIL

ADDRESS CORRECTION REQUESTED

U.S.MAIL

NASA